

# Experimental characterization of aircraft combustor soot: Microstructure, surface area, porosity and water adsorption

O. B. Popovitcheva,<sup>a</sup> N. M. Persiantseva,<sup>a</sup> M. E. Trukhin,<sup>a</sup> G. B. Rulev,<sup>a</sup> N. K. Shonija,<sup>a</sup> Yu. Ya. Buriko,<sup>b</sup> A. M. Starik,<sup>b</sup> B. Demirdjian,<sup>c</sup> D. Ferry<sup>c</sup> and J. Suzanne\*<sup>c</sup>

<sup>a</sup> Moscow State University, 119 899, Moscow, Russia

<sup>b</sup> Central Institute of Aviation Motors, Aviamotornay st. 2, 111250, Moscow, Russia

<sup>c</sup> CRMC2-CNRS, † Département de Physique, Faculté des Sciences de Luminy, Case 901, F-13288 Marseille Cedex 9, France. E-mail: [suzanne@crmc2.univ-mrs.fr](mailto:suzanne@crmc2.univ-mrs.fr)

Received 30th May 2000, Accepted 1st August 2000

First published as an Advance Article on the web 15th September 2000

The laboratory combustion technique operating on a typical combustor of a gas turbine engine is used for soot sampling. Soot particles are derived by combustion of a hydrocarbon  $C_3H_8$ - $n$ - $C_4H_{10}$  mixture at typical cruise conditions. Size, morphology, microstructure, surface area, porosity, and the chemical nature of the soot surface particles are studied by transmission electron microscopy (TEM), Raman and Auger electron spectroscopies (AES), volumetry and gravimetry. Structural irregularities such as micropores determine the specific adsorbability of non-polar gases such as Kr,  $CH_4$  and  $C_6H_6$ . With respect to water adsorption, aircraft combustor soot is far from being hydrophobic. Initial water adsorption on polar heterogeneities leads to pore filling at increasing pressures. The microstructure of soot particles is easily transformed under the influence of adsorbates, giving rise to swelling effects. Due to its specific physico-chemical properties aircraft combustor soot may act as contrail condensation nuclei at low sulfur content in the jet fuel.

## 1. Introduction

There is growing evidence from field observations that a perennial black carbon soot aerosol layer has occurred at 10–11 km altitude.<sup>1,2</sup> A covariance existing between the observed soot mass concentration and calculated fuel usage from air traffic shows that aircraft fuel combustion is the principal source of the soot aerosol layer in the upper troposphere. High emission of soot particles acting as cloud condensation nuclei (CCN) can substantially affect the cirrus formation.<sup>3</sup> Recent studies of Kärcher *et al.*<sup>4</sup> and DeMott *et al.*<sup>5</sup> show that engine soot aerosols as small as 20–60 nm are responsible for ice formation in the aircraft contrail. However, it was hypothesized that fresh exhaust soot particles are hydrophobic.<sup>4–6</sup> Sulfur-induced soot activation models were suggested by Brown *et al.*<sup>6</sup> and Glietsmann and Zellner<sup>7</sup> but they cannot explain the build up of visible contrail at low sulfur level in jet fuel.

To date, most of the model predictions of aircraft soot impact upon the atmosphere are still speculative. Laboratory studies with various carbonaceous materials such as a ground charcoal,<sup>8</sup> amorphous carbon samples,<sup>9</sup> soot from a spark discharge,<sup>10</sup> and *n*-hexane soot,<sup>11</sup> have been undertaken to investigate the soot properties. However, these properties change markedly with the conditions of the soot particles formation.

Aircraft-generated soot particles originate at the specific conditions of high-temperature aviation fuel combustion. A few studies have dealt with the particle size characterization and the nucleation properties of laboratory-simulated jet engine combustor aerosols<sup>12</sup> and exhaust particles,<sup>13</sup> but, adsorbability and heterogeneous reactivity of these kinds of

soot are still underdetermined. Different experimental techniques should be applied for measuring the soot microstructure, porosity, surface area, and the nature of the active sites on its surface.

This paper reports a comprehensive experimental characterization of aircraft combustor soot. The laboratory combustion technique operating on a typical combustor of a gas turbine engine was used for soot production and collection. Different experimental techniques are used to determine the particle size, surface area, porosity, chemical composition and hydrophobicity. Examination of the different results found for carbon black samples is carried out to stress the principal characteristics of aircraft combustor soot.

## 2. Experimental

The combustion chamber of the gas turbine engine at the Central Institute of Aviation Motors (Moscow) has been used to simulate the soot particle emission of aircraft engines. Fig. 1 shows a schematic diagram of a serial aircraft can-annular

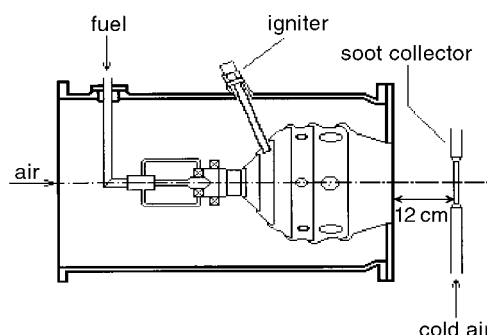


Fig. 1 Combustion chamber of a typical aircraft gas turbine engine with a fuel and air supplying system, and soot sampling.

† Also associated to the Universities of Aix-Marseille 2 and Aix-Marseille 3.

combustor with a fuel and air supplying system, and the soot collector. The combustor has a dome with two coaxial air swirlers having opposite directions for rotation of flows, as is adopted for typical aircraft engines. A gaseous fuel nozzle provides a flow into the inner swirler. The dome generates a system of three coaxial rotating jets of air and fuel in the primary zone of the combustor prior to ignition. This combustor operates on the advanced pre-mixed concept, in the diffusion mode of combustion.

For spraying liquid kerosene, the combustors operate with large air flows and pressures up to 1 MPa. In the present study the combustor incorporates a special system for pre-mixing air with the gaseous hydrocarbon fuel in the primary zone and feeding the combustor with a maximum flow rate at pressures up to 0.4 MPa. This region simulates typical combustion conditions at an average air/fuel equivalence ratio near 4 and a flame temperature in the range 1500–1800 K. The combustion model of Starik *et al.*<sup>14</sup> was considered in order to choose the hydrocarbon fuel used for producing our soot samples. Times of induction and combustion as well as thermal decomposition products, which are responsible for soot formation, were calculated. A mixture of propane–butane (10%) was chosen as a fuel because it showed characteristics similar to typical aviation fuel combustion.

Soot particles were sampled from the post-combustion region on an air-cooled stainless steel probe which was located at a distance of 12 cm from the combustor exit in order to minimize the time of contact with hot exhaust gases. Samples were quickly removed from the probe and transferred in storage tubes, dried at 403 K for 2 h, outgassed, and stored in a fridge.

The size and morphology of the soot particles were examined at CRMC2-CNRS laboratory (Marseille) using a TEM (JEM 2000 FX JEOL (200 kV)) with a resolution of 2.8 Å using the phase-contrast imaging method. A sample of soot particles was dispersed in acetone and a droplet of the mixture was deposited onto a microgrid. The TEM microgrid was previously coated with amorphous carbon with holes of about 10 µm diameter. Soot agglomerates were suspended over the grid holes and were observed without any interference with the underlying substrate. AES was carried out to analyse quantitatively the chemical composition of the soot surface. The Auger spectrometer is a Nanoscan 100 microprofilometer (CAMECA) having an energy resolution of 0.5 eV, a spatial lateral resolution of 1000 Å and a depth profile resolution of 50 Å.

Soot Raman spectra were obtained at Moscow State University (MSU) with a meter monochromator Raman spectrometer (B&M Spectronic BM-100) having a grating with 1200 lines per mm. Measurements were carried out using the 5145 Å line of an 8 mW argon ion laser and scattered radiations were collected in a '180°' configuration. Spectra were recorded in the 568–3900 cm<sup>-1</sup> Stokes range with a resolution of 0.3 Å per channel and a time of accumulation near 4 s per channel.

Gravimetric isotherms were performed at MSU in order to characterize both structural and adsorption soot properties. Benzene molecules, having a diameter of  $d \approx 0.58$  nm, were chosen as a typical adsorbate. However, before adsorbing C<sub>6</sub>H<sub>6</sub>, soot samples were heated at 450 K and outgassed at 10<sup>-5</sup> Torr for 10 h to provide a surface clear from impurities and preadsorbed water.

As graphite is known to be hydrophobic because it shows practically no water adsorption until  $p/p_0$  is close to unity, we used it as a reference sample for studying the relative soot hydrophobicity by performing both gravimetric and volumetric water adsorption isotherms.

Thermodesorption spectrometry of N<sub>2</sub> at room temperature was used to measure the specific surface area of combustor soot after a low-temperature N<sub>2</sub> adsorption for both a reference sample (having a known surface area) and the combustor

soot. Comparison of the integral intensities of the thermodesorption spectra provides us with an estimate of the combustor soot specific surface area. Titration with NaOH and HNO<sub>3</sub> was also performed to estimate the acidic and basic groups concentrations on the soot surface.

Kr and CH<sub>4</sub>, having diameters,  $d \approx 0.36$  and 0.38 nm respectively, were chosen as small model adsorbates to characterize the specific adsorption features of the soot. A conventional volumetric apparatus was used at the CRMC2 laboratory. A thermal pretreatment was carried out by heating samples up to 700 K for 15 h.

### 3. Results and discussion

#### Soot agglomerates: size and morphology

A TEM picture of aircraft combustor soot is shown in Fig. 2 at 60 000 magnification. Soot displays surface irregularities over several length scales. Such 'many-scale' topography is that of a typical fractal agglomerate structure that offers a large specific surface area for adsorption and chemical reactions. One can see in Fig. 2 the spherical-like nature of the soot particles, which have diameters in the 20 to 50 nm range. This is much smaller than thermal carbon black with typical diameters of 200–500 nm and more than that of channel black and carbon aerosols from spark generators. However, the obtained data are very similar to the mean diameters for jet engine aerosols, near 20–50 nm, observed by Petzold *et al.*<sup>12,13</sup> indicating a common way of production.

#### Microstructure

Raman spectroscopy shows us the graphitic nature of soot particles. The Raman spectrum of combustor soot given in Fig. 3 displays the well-known band pair at 1347 and 1595 cm<sup>-1</sup> which is a clear signature of disordered graphitic carbons.<sup>15</sup> The G band (1595 cm<sup>-1</sup>) is attributed to the carbon–carbon stretching vibrations. It is a typical characteristic of a natural graphitic crystal. The D band (1347 cm<sup>-1</sup>) appears in the spectra of small graphitic crystallites and is due to polyaromatic ring vibrations. The D/G band area ratio relates to the graphitic crystallites size,  $L$ . In our case the area ratio is *ca.* 3.3 which corresponds to  $L$  in the 1.2–3 nm range,

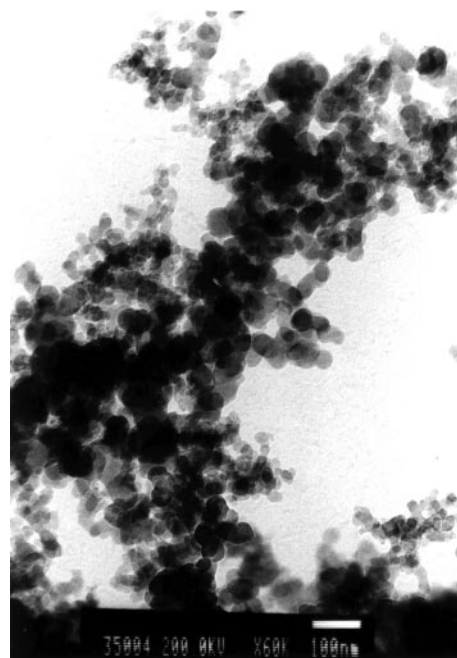


Fig. 2 TEM photomicrograph of combustor soot at 60 000 magnification showing the spherical shape of the soot particles.

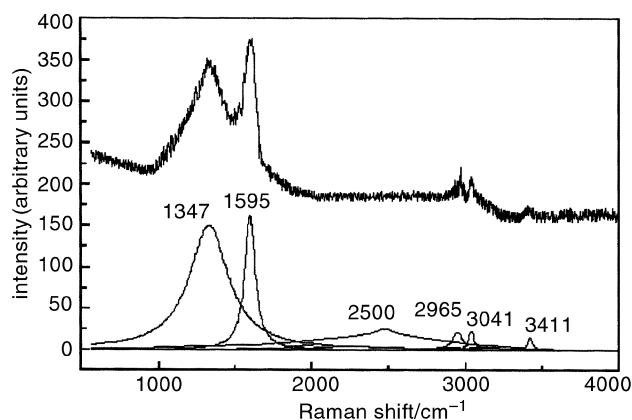


Fig. 3 Raman spectrum of combustor soot.

based on Knight *et al.*<sup>15</sup> and Tuinstra *et al.*<sup>16</sup> The broadening,  $\Delta\nu_G$ , of the G band relates to disorder within the graphite carbon sheet.<sup>15</sup> Various kinds of carbon black (furnace, thermal, channel) show a different degree of order. In our case, the value of  $\Delta\nu_G \approx 86.7 \text{ cm}^{-1}$  is less than  $\Delta\nu_G$  for most disordered graphitic carbon such as charcoal ( $\Delta\nu_G \approx 107 \text{ cm}^{-1}$ ).

In addition, relatively weak bands were observed at 2965 and 3041  $\text{cm}^{-1}$ . They could be due to symmetric and anti-symmetric stretching vibrations of methyl groups  $\nu(\text{CH})$ .<sup>17</sup> The small bands at 3411 and 2500  $\text{cm}^{-1}$  are, respectively, likely to be due to the  $\nu(\text{OH})$  and  $\nu(\text{CO})$  vibrations. Existence of oxygen-containing groups on the surface is also inferred from AES data showing a very important signature of carbon and a small amount (no more than 5%) of oxygen. A 5 keV argon ion bombardment for 2 min on a pressed soot was sufficient to bring about the disappearance of the oxygen signal, meaning that oxygen is present within a surface thickness of about 200 Å.

Our Raman spectroscopy data present a good correlation with TEM microscopy. Fig. 4 shows a phase-contrast image of aircraft combustor soot. One sees that the spherical particles (also called primary particles) are made of carbon layers concentrically arranged in an onion-like structure. Their inner core seems like those observed in Diesel soot by Ishiguro *et al.*<sup>18</sup> The primary particles may be formed by clustering of smaller fine particles, acting as nuclei, on the surface of which graphitic microcrystallites are growing concentrically leading to the onion-like structure. These graphitic microcrystallites have a lateral size of about 2 nm and a thickness of about 3 carbon layers, that is 1 nm. Empty spaces between microcrystallites may arise, particularly close to the particle surface. Slit-like pores could also exist due to the absence of one or more carbon planes. Such a non-perfect surface structure may be a reason for possible structure transformations of soot particles. Moreover, active adsorption sites, which may exist on the edges of the graphitic platelets and inside the pores, can strongly influence the gas adsorption mechanism.

#### Adsorption and porosity

A study of the adsorption properties and porosity of soot particles is primarily based on  $\text{C}_6\text{H}_6$  adsorption-desorption isotherm measurements like those shown in Fig. 5. The dependence of the amount of  $\text{C}_6\text{H}_6$  adsorbed on the relative pressure  $p/p_0$  ( $p_0$  is the saturation vapor pressure) has a wave-like behavior which differs from that observed by Isirikyan and Kiselev<sup>19</sup> with typical graphitized carbon black adsorbents.

Important features like the irreversible adsorption and wide hysteresis loops at low pressure are observed upon the  $\text{C}_6\text{H}_6$  desorption, as shown in Fig. 5. This indicates the existence of micropores and a structural transformation under the influ-

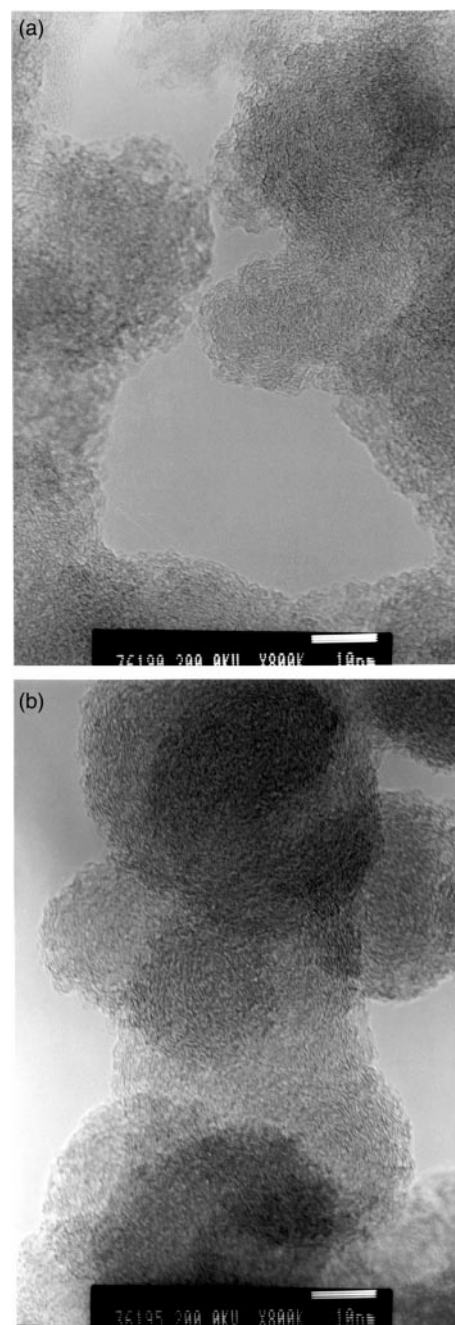


Fig. 4 TEM phase-contrast image of aircraft combustor soot at 800 000 magnification: (a) Microstructure of an aircraft combustor soot particle showing interparticle mesopores. (b) Some aircraft combustor soot particles showing the concentrically onion-like oriented graphite planes.

ence of the adsorbate.<sup>20</sup> The slit-like nature of the micropores may be inferred from the shape of the desorption isotherm which is nearly horizontal. The  $\text{C}_6\text{H}_6$  molecules trapped in the carbon interlayer space may diffuse out slowly and, at very low  $p/p_0$  values, a significant amount of  $\text{C}_6\text{H}_6$  molecules remaining in the soot micropores are removed only by heating up to 753 K.

The specific surface area, determined by using the BET equation, is  $S \approx 32 \text{ m}^2 \text{ g}^{-1}$  if small relative pressures up to  $p/p_0 \approx 0.1$  are taken into account and it increases up to  $48 \text{ m}^2 \text{ g}^{-1}$  in the 0.2 to 0.38  $p/p_0$  range. It looks as if the  $\text{C}_6\text{H}_6$  molecules increase the size of the micropores when they penetrate them at increasing pressure.

The noticeable structure transformation described above is known as the “swelling” phenomenon.<sup>20</sup> Existence of this phenomenon is supported by the increasing amount of  $\text{C}_6\text{H}_6$

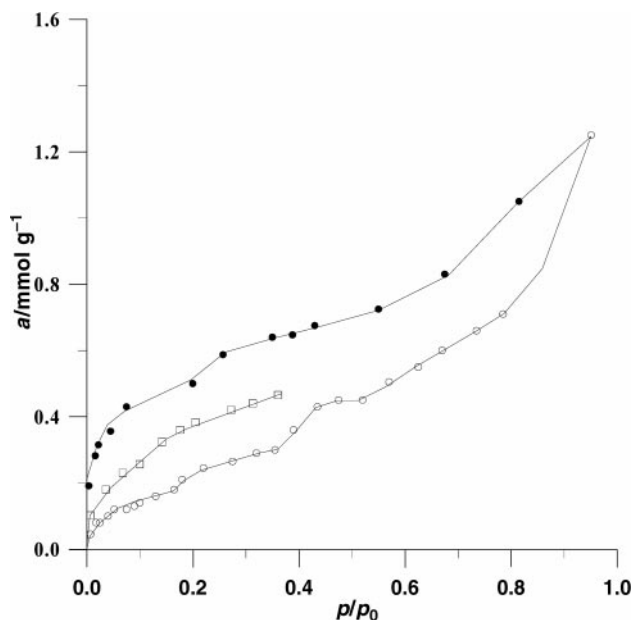


Fig. 5 Adsorption-desorption isotherms of  $C_6H_6$  on combustor soot: (○) first cycle, (□) second adsorption. Open symbols: adsorption; filled symbols: desorption.  $T = 298$  K.

adsorbed during the second repeated adsorption performed after a previous adsorption-desorption cycle, as shown in Fig. 5.

The swelling of the soot under the influence of  $C_6H_6$  adsorption has to be correlated with the large diameter of the  $C_6H_6$  molecules which penetrate the narrow pores, transforming their structure. An analysis of the  $CH_4$  and Kr adsorption isotherms has been undertaken to see if this effect is also observed for smaller molecules than  $C_6H_6$ .

Adsorption-desorption isotherms of  $CH_4$  and Kr are shown in Fig. 6. The first measurement for a given soot sample was the  $CH_4$  adsorption-desorption cycle. The adsorption isotherm is initially convex in the 0–0.02 relative pressure range, which indicates a strong attractive interaction between adsorbed molecules and adsorbent, probably in

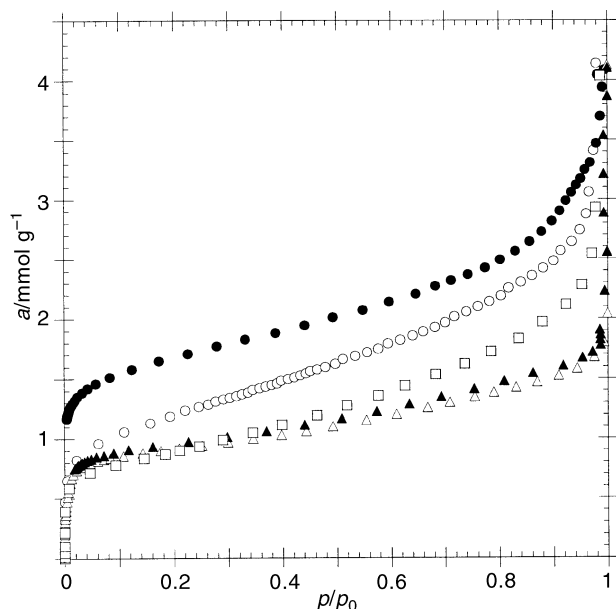


Fig. 6 Adsorption-desorption isotherms on combustor soot for: (○)  $CH_4$ , (△) Kr, (□) second adsorption of  $CH_4$ . Open symbols: adsorption; filled symbols: desorption.  $T = 77$  K.

micropores having sizes of several times the diameter of the methane molecule.

The Dubinin-Radushkevich equation for micropore volume filling has been applied to our  $CH_4$  adsorption data:

$$\log W = \log W_0 - D(\log p_0/p)^2 \quad (1)$$

where  $W_0$  is the total volume of micropores,  $D$  is a Dubinin's theory parameter that is  $T^2(K/\beta^2)$  where  $K$  is a constant related to the adsorption potential distribution and  $\beta$  is the affinity coefficient of the adsorbate.<sup>21</sup> We estimate the total volume of micropores to be  $W_0 = 0.036$   $cm^3$   $g^{-1}$  by considering the 0–0.02 relative pressure range. This has to be compared to the  $W_0$  values of natural coal and active black carbons which are in the 0.15–0.5  $cm^3$   $g^{-1}$  range.

A further increase in the  $CH_4$  relative pressures above 0.02 suggests that capillary condensation into mesopores of larger size and/or multilayer condensation occur(s). The total volume of mesopores can be estimated using data in the 0.2–0.95 relative pressure range. We find a value close to 0.064  $cm^3$   $g^{-1}$  if we assume a  $CH_4$  density of 0.466  $g$   $cm^{-3}$  at 77 K. Fig. 4 suggests to us that the cavities between primary particles may be soot mesopores.

Following our experiments with  $CH_4$ , we have performed Kr adsorption-desorption cycles on the same soot. Note that the structure of this soot has already been transformed by the previous  $CH_4$  adsorption. Unlike in the case of methane, we do not observe a wide hysteresis. Nevertheless, we note that the specific surface area was reduced from 100  $m^2$   $g^{-1}$  for the fresh soot sample to 71  $m^2$   $g^{-1}$ . A structure modification could explain the decrease in the amount of adsorbed  $CH_4$  at the second adsorption as shown in Fig. 6. It should be noted here that the soot structure evolution upon adsorption of  $CH_4$  and Kr is opposite to that observed with benzene, *i.e.* a surface area decrease in the case of  $CH_4$  and Kr compared to an increase for  $C_6H_6$ . The origin of this difference is not known.

#### Adsorption of water

Adsorption of water vapor by carbon blacks involves a distinctively different mechanism from the adsorption of simple non-polar molecules. An adsorption isotherm of water on combustor soot with  $S \approx 47$   $m^2$   $g^{-1}$  is shown in Fig. 7. In the initial  $p/p_0$  region, the isotherm is concave to the pressure axis which is typical for weak adsorbate-adsorbent interactions. The adsorption is likely to be due to active oxygen groups

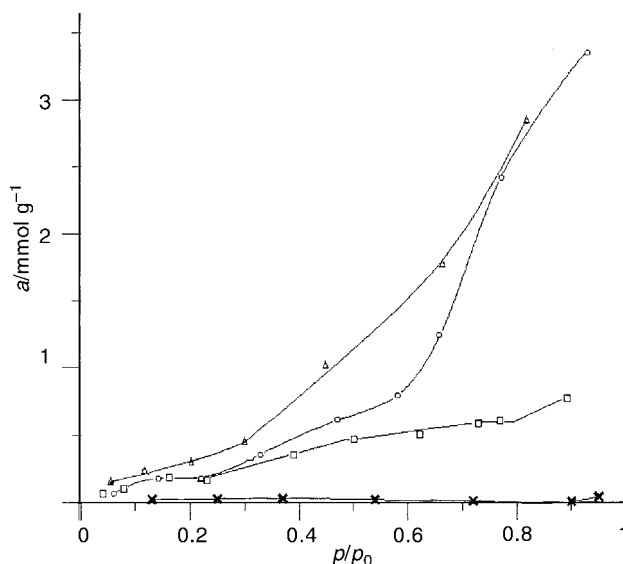


Fig. 7 Adsorption isotherm of water on combustor soot at 295 K, (×) graphite at 300 K, (□) combustor soot after  $C_6H_6$  adsorption at 298 K, (△) after one water adsorption-desorption cycle at 295 K.

which may act as primary adsorption sites.<sup>20</sup> A titration experiment shows that the amounts of acidic and basic groups on the combustor soot surface are, respectively, less than 0.1 and 0.02 mmol g<sup>-1</sup>. These values are in good correlation with a small amount of water adsorbed in the initial pressure regime.

The isotherm on combustor soot rises slowly until  $p/p_0 \approx 0.6$ , probably because of water adsorption on previously primarily adsorbed water molecules which act as secondary adsorption centers. The steep rise in the adsorbed water amount on the combustor soot at  $p/p_0 \geq 0.6$  is similar to the water specific behavior on natural porous coals.<sup>20</sup> It may be explained by the formation of water clusters which leads to rapid micropore filling. However, due to the soot surface heterogeneities, mesopores may also play a role in water adsorption through capillary condensation and/or multilayer adsorption. But the steep rise is not observed for the water adsorption isotherm on combustor soot after a previous C<sub>6</sub>H<sub>6</sub> adsorption–desorption cycle, as shown in Fig. 7. This latter finding is associated with the size modification of the micropores by C<sub>6</sub>H<sub>6</sub>.

A comparative analysis of aircraft combustor soot hydrophobicity can be performed based on water adsorption on graphite. A water adsorption isotherm on a graphite sample having a specific surface area of  $S \approx 20 \text{ m}^2 \text{ g}^{-1}$  is shown in Fig. 7. The amount of adsorbed water at low  $p/p_0$  on combustor soot is more than 60 times that on graphite, showing once more that the surface active sites play a significant role in determining the adsorption behavior.

After a first water adsorption–desorption cycle on combustor soot some water molecules may remain strongly adsorbed onto the surface. Fig. 7 shows the second water adsorption isotherm carried out after the first adsorption–desorption cycle and an outgassing at 450 K for 2 h. It is clear that this treatment cannot remove strongly adsorbed water molecules, suggesting a close connection between water retention and the presence of additional surface active sites. Additionally, an increase in the specific surface area during water adsorption may take place related to swelling effects. It is confirmed by the specific surface area measurements made before and after the adsorption which provide  $S \approx 52 \text{ m}^2 \text{ g}^{-1}$  and  $S \approx 76 \text{ m}^2 \text{ g}^{-1}$ , respectively. However, we should note that significant transformations of the properties of soot under water adsorption were observed only for relative pressures close to unity. This observation has to be taken into account for soot ageing considerations. In this context, we have studied the amount of adsorbed water on a reference sample which has been stored for 6 months at ambient conditions without any pretreatment and outgassing. In the initial relative pressure range (which is more sensitive to oxidation processes), we found an adsorbed water amount increase of 10% over that on a soot sample stored in conditions described in Section 2. This shows that if soot samples are stored without being exposed to a nearly water-saturated atmosphere, their structure and adsorptive properties will not be dramatically affected.

## Conclusions

We have shown that the soot produced by a gas turbine engine combustion chamber demonstrates specific features. We have used various experimental techniques: adsorption isotherm measurements, Raman and AES, TEM and titration, which allow characterization of the hydrocarbon soot particles and the prominent role of their microstructures on the adsorption properties. The soot is composed of agglomerates of spherical particles having diameters within the 20–50 nm range and is best described as fractal clusters. Due to the short time of formation during the hydrocarbon fuel combustion, soot particles feature disordered graphitic microcrystallites

arranged in concentric layers leading to an onion-like structure. These microcrystallites have sizes of about 2 nm with micropores situated in the slits between graphite planes. Furthermore, some crystalline imperfections may appear during the formation of the particles and mesopores are formed due to spaces between the particles. The specific surface area ranges from 47 to 100 m<sup>2</sup> g<sup>-1</sup>, directly related to the surface area of pores.

The soot microstructure plays a prominent role in the adsorption properties of simple non-polar molecules such as hydrocarbons and Kr. The mechanism of their adsorption is pore filling related to strong attractive interactions inside the micropores. Hence, the classical Langmuir theory of layer-by-layer filling is not applicable. The microstructure of aircraft combustor soot particles is easily transformed under the influence of adsorbed molecules leading to a surface area change. C<sub>6</sub>H<sub>6</sub> and CH<sub>4</sub> molecules, which have been used in this study, produce such a surface area modification.

The behavior of water adsorbed on combustor soot is of particular interest. It features an enhanced water adsorption at low relative pressures compared with hydrophobic graphite due to the existence of polar heterogeneities at the soot surface. Combustor soot adsorbs about 10<sup>-4</sup> g H<sub>2</sub>O m<sup>-2</sup> of soot surface at a relative humidity of 10%. This corresponds approximately to 0.25 of an equivalent surface monolayer if we assume a water molecule surface area of  $\approx 0.1 \text{ nm}^2$ . Cooperative pore filling may be a possible mechanism for water adsorption when the pressure is increased and water clusters are likely to be formed. This mechanism is deeply relevant to the formation of embryonic water droplets and heterogeneous nucleation on aircraft exhaust soot particles in the atmosphere.

Frequent changes of the relative humidity in the real atmosphere give rise to numerous water adsorption–desorption (condensation–evaporation) cycles on the soot particles. For hydrocarbon combustor soot, contact with a saturated water vapor atmosphere produces a permanent change in the surface properties, reducing its hydrophobicity. Our results provide strong evidence for irreversible chemisorption and ageing of soot particles in the atmosphere, *i.e.* more favorable conditions for soot hydration and CCN formation.

Finally, it is important to note that during the combustion of real aviation fuel containing sulfur impurities, the soot particles may acquire a certain sulfur mass fraction which can influence their ice nucleating properties. The results presented here correspond to the lower limit of water adsorption on aircraft soot. In the light of the conclusion that “pure” aircraft combustor hydrocarbon soot is far from being hydrophobic, its specific physico-chemical characteristics should be included in the evaluation of the potential of aircraft soot to act as contrail condensation nuclei at low sulfur content in jet fuel.

## Acknowledgements

Financial support partially from EC Environmental and Climate project, contract No. CT97/0620 and Russian Fond of Basic Research, contract No. 00 1596554 and No. 98 0217332 is gratefully acknowledged.

We also wish to thank S. Nitsche for his help in the TEM measurements and A. Baronnet and S. Giorgio for fruitful discussions and suggestions about the interpretation of the TEM images.

## References

- 1 D. F. Blake and K. Kato, *J. Geophys. Res.*, 1995, **100**, 7195.
- 2 A. W. Strawa, K. Drdla, G. V. Ferry, S. Verma, R. F. Pueschel, M. Yasuda, R. J. Salawich, R. S. Gao, S. D. Howard, P. T. Bui, M. Loewenstein, J. W. Elkins, K. K. Perkins and R. Cohen, *J. Geophys. Res.*, 1999, **104**, 26753.
- 3 J. H. Seinfeld, *Nature*, 1998, **391**, 837.

- 4 B. Kärcher, T. Peter, U. M. Biermann and U. Schumann, *J. Atmos. Sci.*, 1996, **53**, 3066.
- 5 P. J. DeMott, Y. Chen, S. M. Kreidenweis, D. C. Rogers and D. E. Sherman, *Geophys. Res. Lett.*, 1999, **26**, 2429.
- 6 R. C. Brown, R. C. Miakelye, C. E. Kolb and T. J. Resch, *J. Geophys. Res.*, 1996, **101**, 22939.
- 7 G. Gleitsmann and R. Zellner, *J. Geophys. Res.*, 1998, **103**, 19543.
- 8 L. Brouwer, M. J. Rossi and D. M. Golden, *J. Phys. Chem.*, 1986, **90**, 4599.
- 9 C. A. Rogaski, D. M. Golden and L. R. Williams, *Geophys. Res. Lett.*, 1997, **24**, 381.
- 10 S. Kamm, O. Mohler, K.-H. Naumann, H. Saathoff and U. Schurath, *Atmos. Environ.*, 1999, **33**, 4651.
- 11 D. M. Smith and A. R. Chughtai, *J. Geophys. Res.*, 1996, **101**, 19607.
- 12 A. Petzold and F. P. Schröder, *Aerosol. Sci. Technol.*, 1998, **28**, 62.
- 13 A. Petzold, J. Ström, F. P. Schröder and B. Kärcher, *Atmos. Environ.*, 1999, **33**, 2689.
- 14 A. M. Starik, N. S. Titiva and L. F. Yanovski, *High Temp.*, 1999, **37**, 270.
- 15 D. S. Knight and W. B. White, *J. Mater. Res.*, 1989, **4**, 385.
- 16 F. Tuinstra and J. L. Koenig, *J. Chem. Phys.*, 1970, **53**, 1126.
- 17 J. Bullo and M. P. Schmidt, *Phys. Status Solidi B*, 1987, **143**, 345.
- 18 T. Ishiguro, Y. Takatori and K. Akihama, *Combust. Flame*, 1997, **108**, 231.
- 19 A. A. Isirikyan and A. V. Kiselev, *J. Phys. Chem.*, 1962, **66**, 205.
- 20 S. J. Gregg and K. S. W. Sing, in *Adsorption, Surface Area and Porosity*, Academic Press, New York, 2nd edn., 1982.
- 21 M. M. Dubinin, in *Chemistry and Physics of Carbon*, ed. P. L. Walker, Marcel Dekker, New York, 1965, vol. II.